# Support Information
# Microrail-Assisted Liposome Trapping and Aligning in Microfluidic Channels

Shun Okada and Kan Shoji*

Department of Mechanical Engineering, Nagaoka University of Technology, 1603-1 Kamitomioka, Nagaoka, Niigata 940-2188, Japan

* Corresponding authors

E-mail: kshoji@mech.nagaokaut.ac.jp (K.S.)

Content:

## S.1. Preparation of liposomes

Liposomes were prepared using the water-in-oil (w/o) emulsion transfer method (Fig. S2). Briefly, DOPC was mixed with the Chol in the chloroform. The chloroform was evaporated using nitrogen gas and dissolved in mineral oil to prepare 13 mM lipid solution (10 mM DOPC and 3 mM Chol). Next, 20 μL inner solution (500 mM sucrose and 100 μM calcein) was added to 200 μL lipid solution, and w/o emulsions were produced by tapping the microtube containing the mixed solution approximately 10–20 times. The solution was then incubated on ice for 15 min. Similarly, 100 μL lipid solution was added on top of 200 μL outer solution (500 mM glucose), and the mixture was incubated at 4°C for 15 min. Subsequently, 220 μL w/o emulsion solution was gently added to the lipid solution on top of the outer solution and centrifuged at 8000 *g* for 15 min at 4°C. The liposome pellet was collected by removing the supernatant, and 200 μL outer solution was added to the pellet. Liposomes containing 50 μM Liss-Rhod-PE in the membrane lipids were prepared for z-stack imaging of liposomes trapped under the microrail. To prevent infusing lipid debris into the microchannel, we initially incubated the liposome solution for one hour and waited until the lipid debris accumulated at the bottom. Then, we collected the supernatant of the solution with a pipette and used it.

## S.2. Effect of the main channel height

When the flow distributions were compared between the different main channel heights of the microrail channel, the region of high flow velocity moved in the microrail when the main channel height decreased to 15 μm. The ratio of the main channel and microrail flow rates can be calculated using the fluidic resistance ratio. The equation of the fluidic resistance ratio derived from the Darcy–Weisbach equation was used for channels with completely separate main and subchannels, as described previously.[1] Using the Darcy–Weisbach equation, the pressure drop $\Delta p$ in the microrail channel can be expressed as follows:

$$\Delta p = \frac{C(\alpha)\mu L Q P^2}{32 \quad A^3} \#(1),$$

where $C(\alpha)$ is a constant that is a function of the aspect ratio α; μ is the fluid viscosity; $L$ is the length of the channel; $Q$ is the volumetric flow rate; and $P$ and $A$ are the perimeter and area of the channel, respectively. The aspect ratio is defined as the height divided by the width of the channel. When the geometric structure parameters of the microrail channel are considered, the fluidic resistance ratio $R_m / R_r$ between the main channel and microrail can be expressed only as the geometric dimensions of the microrail channel:

$$\frac{R_m}{R_r} = \frac{Q_r}{Q_m} = \left(\frac{C_r(\alpha)}{C_m(\alpha)}\right) \cdot \left(\frac{w_r(h_r + h_m)}{w_m h_m}\right)^3 \cdot \left(\frac{w_m + h_m}{w_r + (h_r + h_m)}\right)^2 \#(2),$$

where $w$ and $h$ denote the channel width and height, respectively; and subscripts $m$ and $r$ denote the main channel and microrail, respectively. In this study, because the main channel width was constant, we found that the ratio of the main channel and microrail flow rates is determined by the relationship between the main channel height and microrail width. When the main channel width was 100 μm, the $R_m / R_r$ at $h_m$ = 10, 15, 20, 30, 40, and 50 μm were 3.01, 1.28, 0.75, 0.44, 0.36, and 0.32, respectively.

The ratio of the main channel and microrail volumetric flow rates was also analyzed in the simulation. The volumetric flow rate of the microrail channel decreased with increasing main channel height. Thus, the

ratios of the volumetric flow rate $Q_r/Q_m$ at $h_m$ = 10, 15, 20, 30, 40, and 50 μm were 2.62, 1.03, 0.56, 0.27, 0.17, and 0.12, respectively (Fig. S4).

In the analysis, the flow velocity in the main channel region was faster at $R_m / R_r > 1$ and slower at $R_m / R_r < 1$ than that in the microrail region. Because $R_m / R_r < 1$ at a main channel height < 15 μm, the results agreed with the flow distribution simulation (Fig. S3). Furthermore, comparing the calculated and simulation values showed that both values generally matched, indicating that the change in the flow rate ratio depends on the fluidic resistance ratio. Hence, the proposed equation of the fluidic resistance ratio can be applied to determine the region of high flow velocity. However, all the simulation values were larger than the calculated values. Compared with previous findings[1], the main channel region overlapped with a part of the microrail region in the microrail channel. In the simulation, the main channel and microrail regions affected each other. Thus, the simulation values obtained were larger than the calculation values.

Reference:

1 W. H. Tan and S. Takeuchi, *Proc. Natl. Acad. Sci. U. S. A.*, 2007, **104**, 1146–1151.

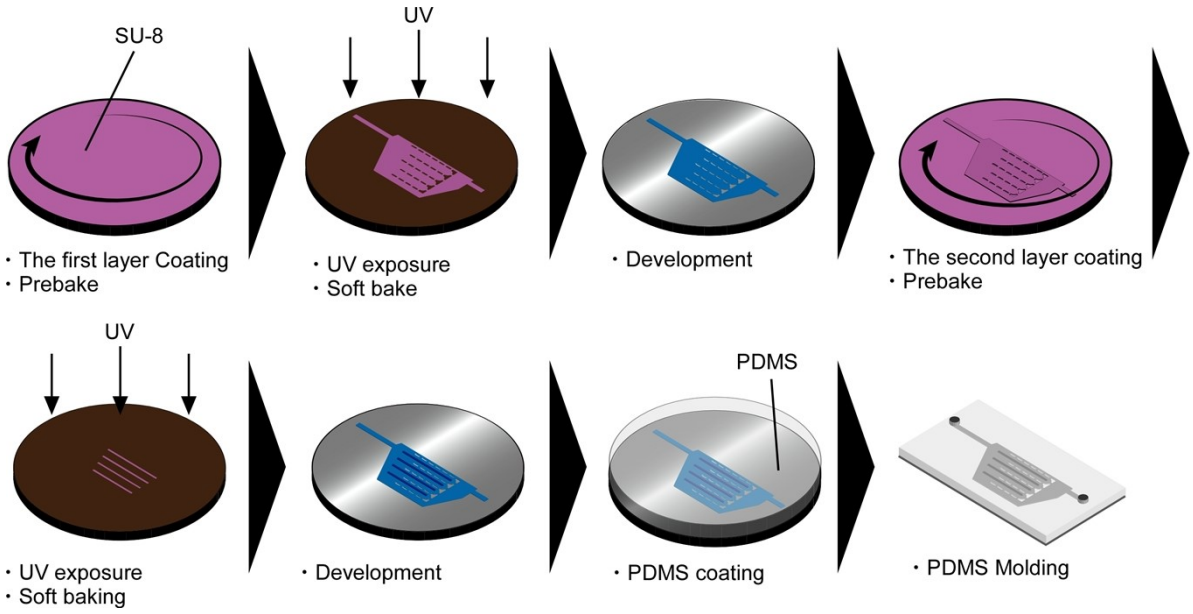


Fig. S1 Fabrication processes of microrail devices.

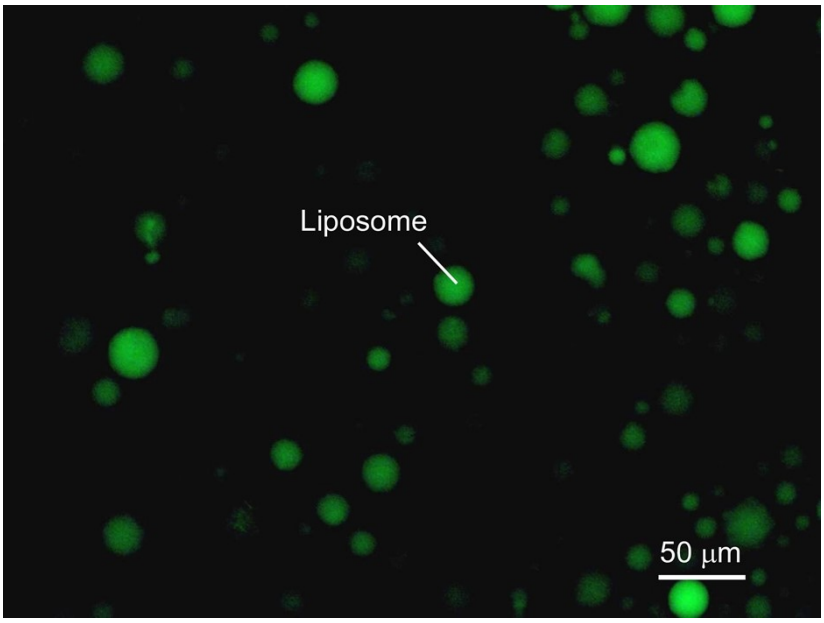


Fig. S2 Fluorescent image of liposomes.

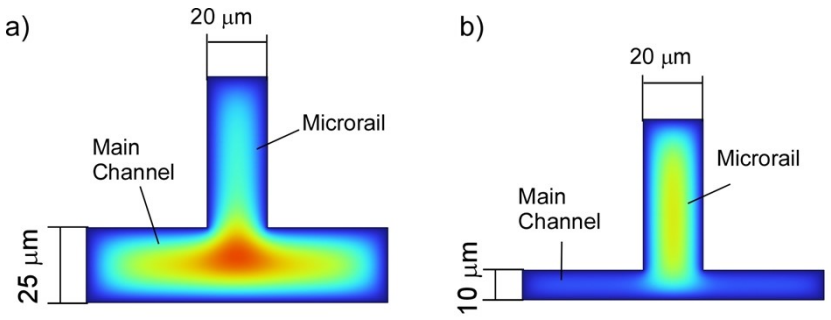


Fig. S3 Flow distributions in the cross-section of the microrail channel with the main channel heights of a) 25 and b) 10 μm.

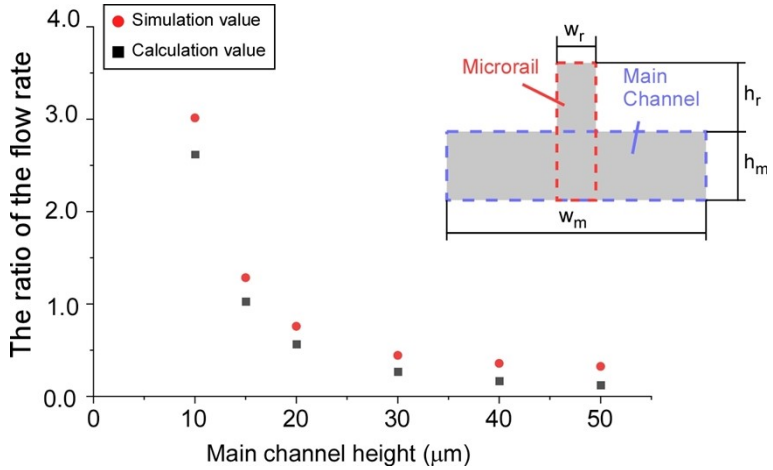


Fig. S4 Variation of the flow rate ratios with main channel height $h_m$. Constant parameters: $w_m$= 100μm, $L_m$= 1000 μm, $w_r$= 30 μm, $h_r$= 50 μm, $L_r$= 500 μm.

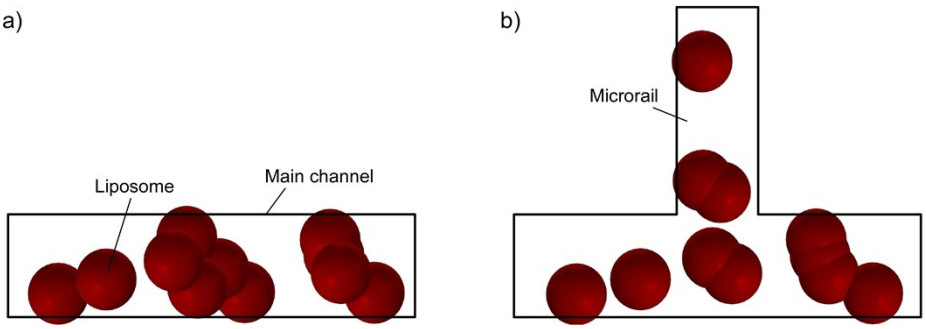


Fig. S5 Movement of ten liposomes in the microrail channel. The liposome positions at a) inlet and b) outlet.

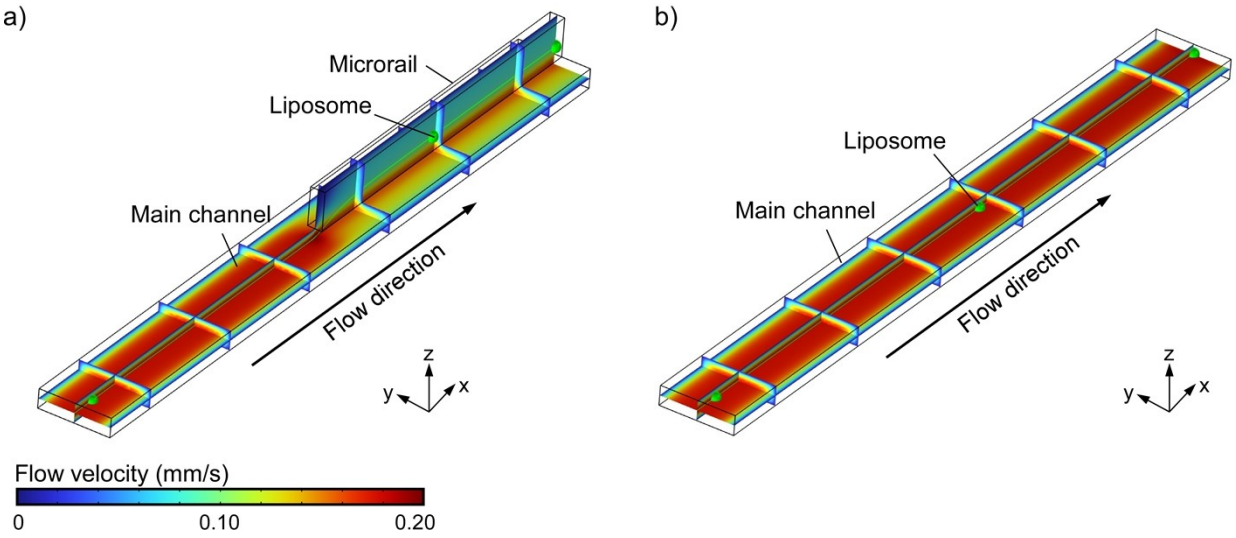


Fig. S6 Trajectories of liposomes with 15 µm diameter in a) the microrail microchannel and b) the rectangular channel. The flow rate was 0.1mm/s. Geometric parameters: $w_m$= 100µm, $L_m$= 1000 µm, $h_m$=25 µm.

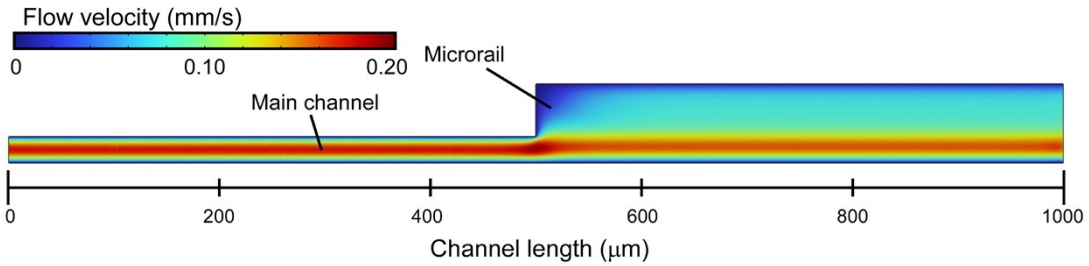


Fig. S7 Flow distribution of the cross-section on the x-z plane of the microrail channel.

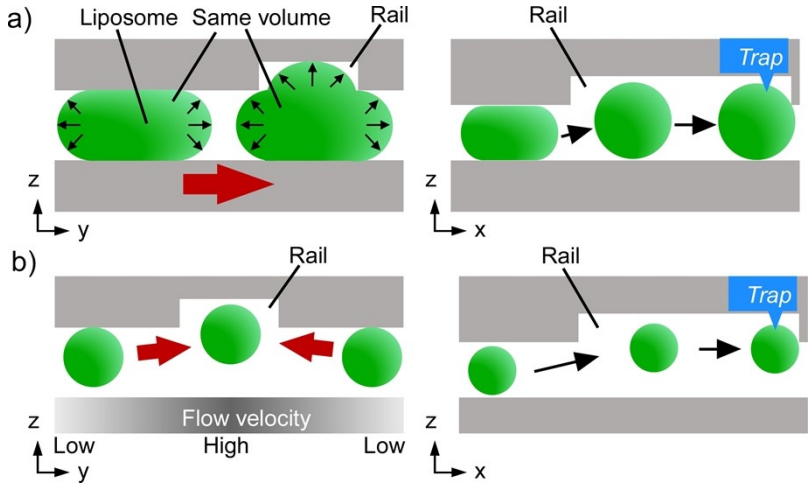


Fig. S8 Suggested mechanisms of liposomes trap by a) surface energy and b) drag force.


Fig. S9 Design of a) the main channel and b) the microrail layers of the microrail device. All scale

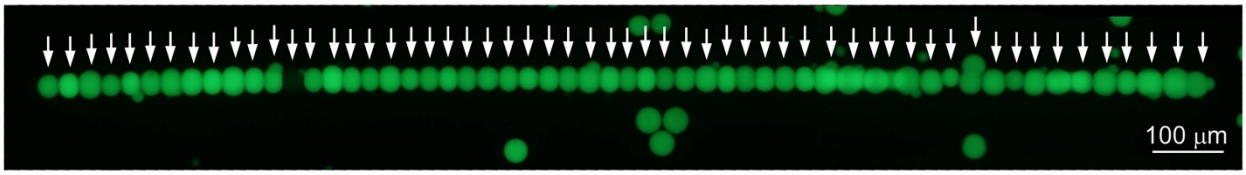


Fig. S10 Microscopic image of the 57 liposomes aligned under the microrail.

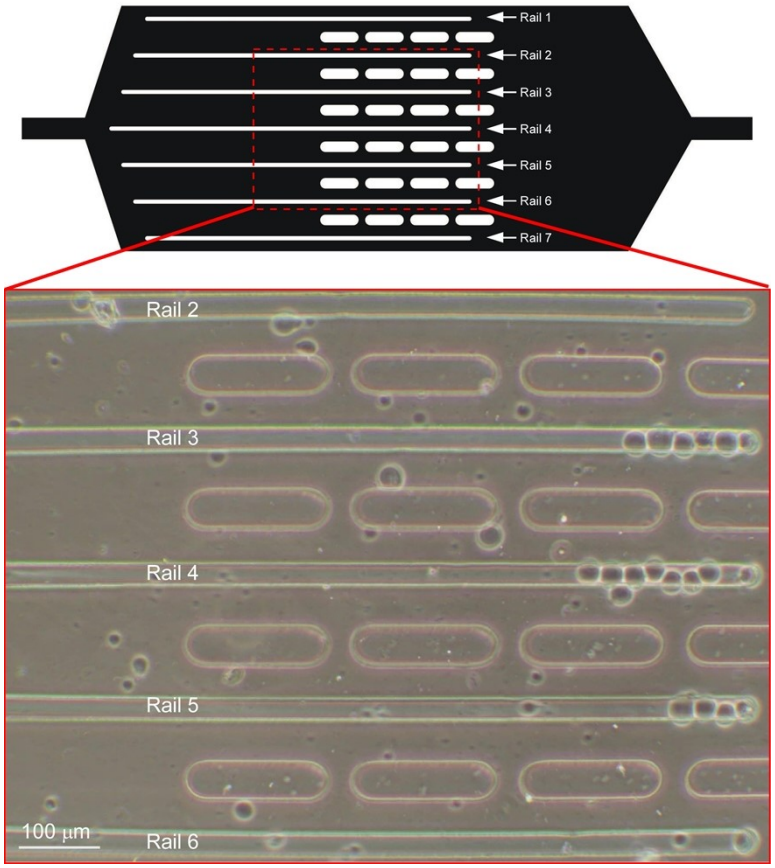


Fig. S11 Microscopic image of the liposomes trapped in the microraill device.

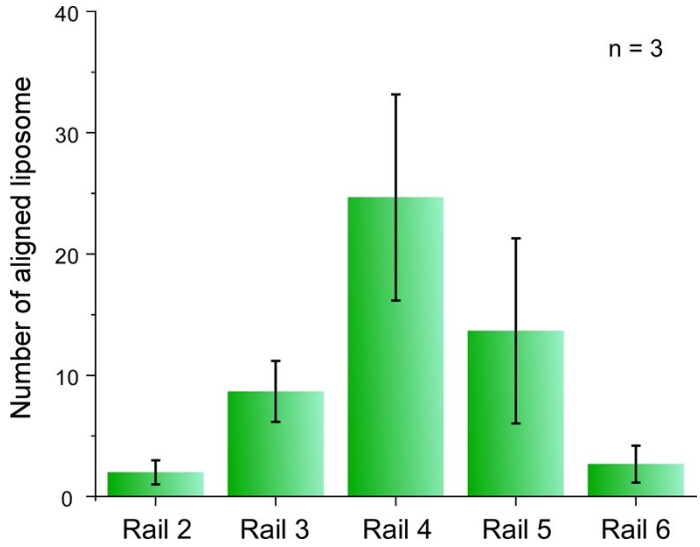


Fig. S12 Number of aligned liposomes under the microrails (Nos. 2, 3, 4, 5, and 6) at 60 min after the first liposome was trapped. Liposomes trapped under the outer microrails (Nos. 1 and 7) could not be analyzed because these microrails were out of field of view.

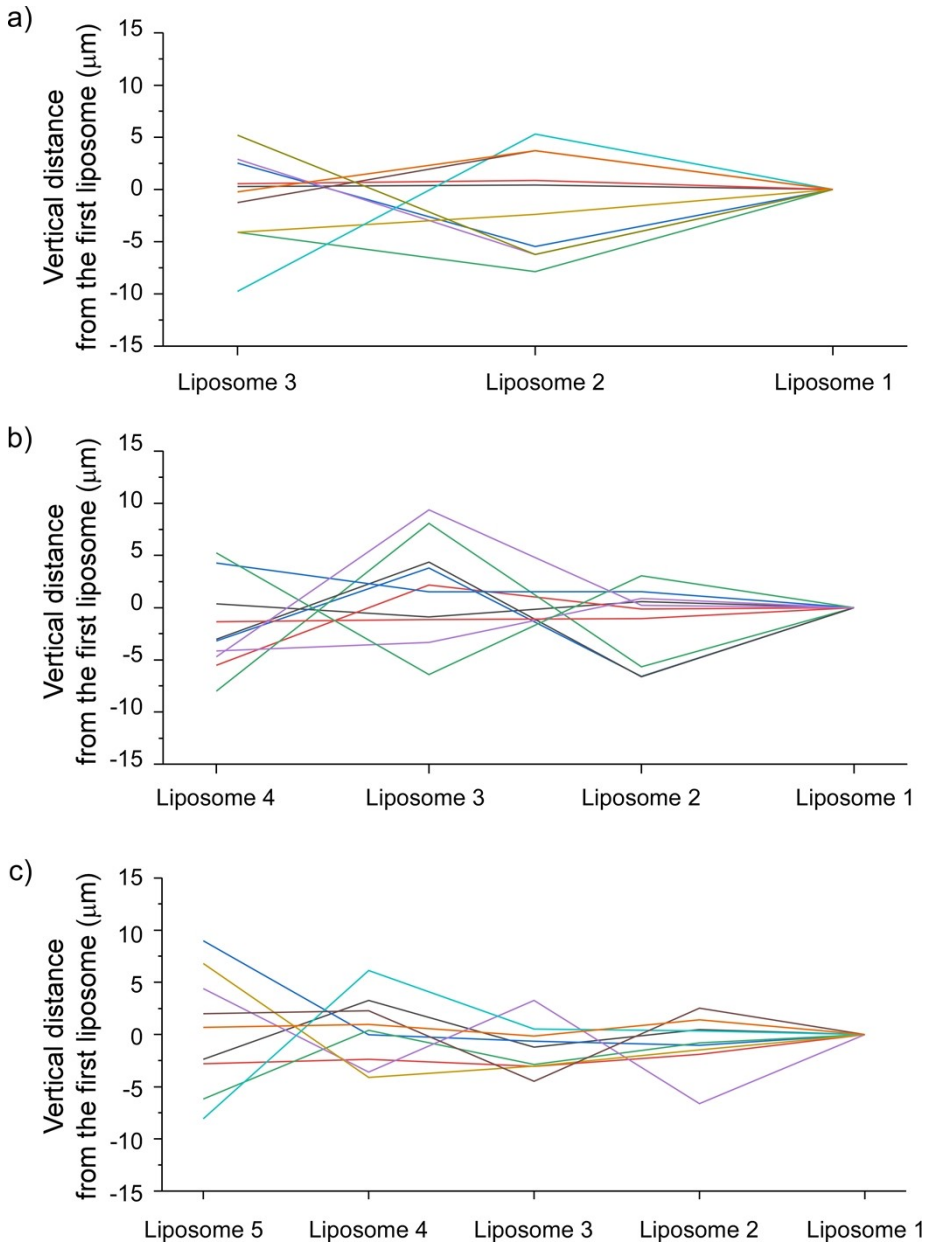


Fig. S13 Vertical distances between each trapped liposome and the first liposomes. We evaluated the cases that a) three, b) four, and c) five liposomes were aligned under the microrails.

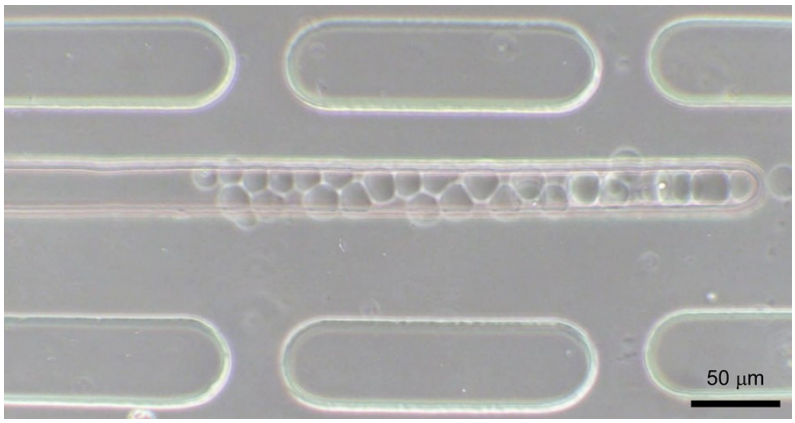


Fig. S14 Microscopic image of trapped liposomes in the microrail device with 10 μm of the main channel height. The liposomes were not aligned in a row because the size of the trapped liposome was smaller than the microrail width.

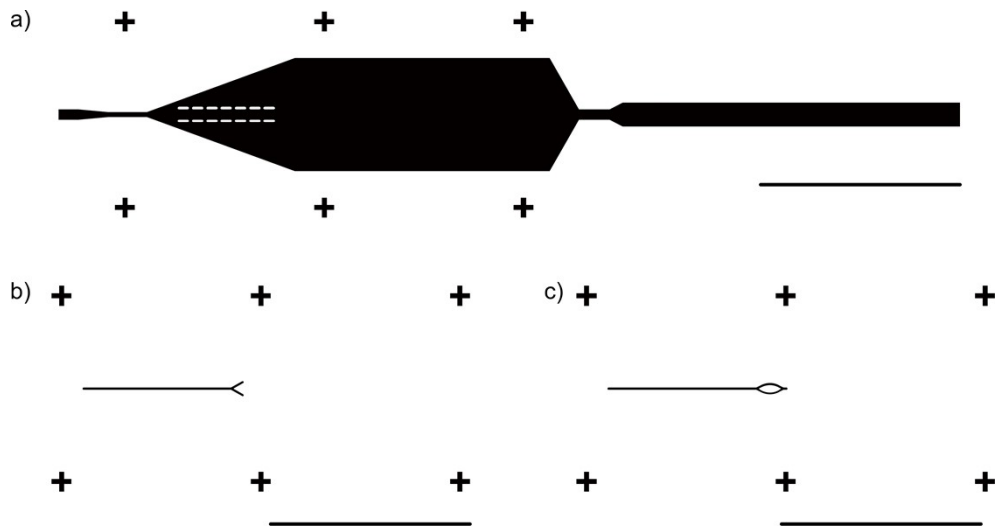


Fig. S15 Designs of a) the main channel, b) the y-shaped microrail, and c) ring-shaped microrail. All scale bars are 2 mm.